Paper CFDSC-2013 #178, Session 13–6 - Rotating Machine I,
21st Annual Conference of the CFD Society of Canada,
Sherbrooke, Canada, May 6–9, 2013.

Parametric study of H-Darrieus vertical-axis turbines using uRANS simulations

Rémi Gosselin[1], Guy Dumas, and Matthieu Boudreau

Laboratoire de Mécanique des Fluides Numérique, Département de génie mécanique
Université Laval, Québec, Québec, G1V 0A6, Canada

Email: *remi.gosselin.2@ulaval.ca*

Abstract

A parametric study of vertical axis turbines is conducted using the k-ω SST RANS model in its unsteady form. The effect of solidity, number of blades, Reynolds number, blade pitch angle (fixed and variable) and blade thickness on the aerodynamic efficiency of the turbine is evaluated in order to determine what would be the best aerodynamic configuration in a given application. The impact of 3D effects associated to the blade aspect ratio and the use of end-plates is also investigated. Optimal radius-based solidity is found to be around $\sigma = 0.2$, but higher solidity turbines can have their performance improved by pitch control. Variable pitch functions allow up to 27% relative gain in efficiency, coming close to the Betz limit for the 2D case. In 3D, a small blade aspect ratio ($AR = 7$) leads to a relative efficiency drop of 60% compared to the 2D prediction. Longer blades improve the 3D efficiency greatly. End-plates are found to have a positive effect on power extraction performance, as long as their size is limited.

Nomenclature

α	Blade angle of attack, see Fig. 2b
α_0	Blade pitch angle, see Fig. 2b
α_{cst}	Target angle of attack for variable pitch control
β	Force angle, see Fig. 2b
η	Turbine efficiency ($\eta = \overline{C_P}$)
λ	Blade Tip Speed Ratio (TSR)
ν	Fluid kinetic viscosity
ω	Turbine rotational speed ($\omega = \frac{d\theta}{dt}$)
ρ	Fluid density
σ	Solidity based on turbine radius
θ	Azimuth angle
A	Swept area of the turbine ($2R \times H$ in the case of a H-Darrieus turbine)
AR	Blade Aspect Ratio $AR = \frac{H}{c}$
c	Blade chord length
C_P	Instantaneous power coefficient, ratio of power extracted to power available, see Eq. 1
$\overline{C_P}$	Cycle-averaged power coefficient, see Eq. 2
D	Drag force on a blade
F_N	Normal force on a blade
F_T	Tangential force on a blade
H	Turbine height
L	Lift force on a blade
M	Moment around the turbine axis of rotation
N	Number of blades
R	Turbine radius
Re	Reynolds number based on average blade speed
U_∞	Free stream velocity

1 Introduction

The vertical-axis turbine (VAT; wind turbine: VAWT; or hydrokinetic turbine: VAHT) principle was proposed by George Darrieus in the 30s, but has not been developed since then as much as horizontal-axis turbines (HATs), despite many interesting characteristics.

The main advantage of VATs compared to HATs is that they are axisymmetric, meaning that an orientation mechanism is not needed whatever the upstream flow direction. On the other hand, vibrations induced by the non-constant forces on the blades lead to a real mechanical challenge and one of the main reasons why this design principle is not as popular among current turbine manufacturers.

The power extraction performance of a VAT is governed by the following 2D parameters:

- Blade profile and chord (c)
- Number of blades: N
- Solidity based on the turbine radius: $\sigma = \frac{Nc}{R}$
- Tip speed ratio (TSR): $\lambda = \frac{R\omega}{U_\infty}$
- Reynolds number based on blade rotational speed: $Re = \frac{R\omega c}{\nu}$.

There are also various 3D parameters that influence the aerodynamic efficiency, among which:

- Blade aspect ratio: $AR = \frac{H}{c}$
- Blade configuration (straight blade, helix, “eggbeater", canted...)
- Presence and shape of end-plates.

The power coefficient C_P is defined as the ratio of the power extracted to the power available.

$$C_P(\theta) = \frac{M(\theta)\omega}{\frac{1}{2}\rho U_\infty^3 A} \quad . \tag{1}$$

The aerodynamic efficiency of the turbine $\overline{C_P}$ is given by the average power coefficient C_P over one revolution.

$$\eta \equiv \overline{C_P} = \frac{1}{2\pi}\int_0^{2\pi} C_p(\theta)d\theta \quad . \tag{2}$$

Different geometric parameters, force components and angles are also defined in Figs. 1, 2a and 2b.

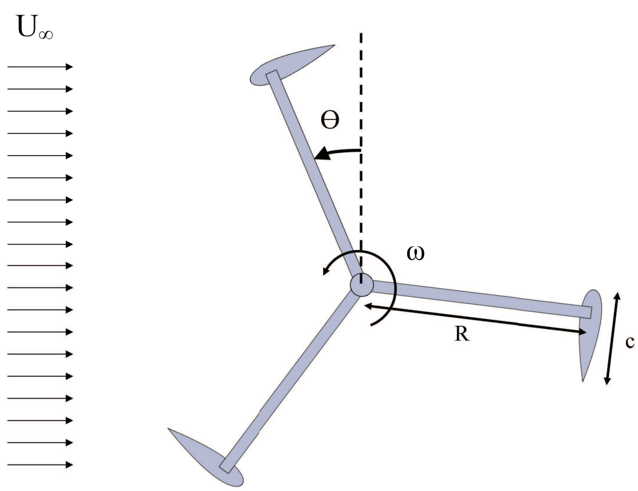

Figure 1: *Different geometric parameters and azimuth angle (θ) of a Darrieus turbine.*

Simulation of such turbines over a vast range of TSR is challenging, because the aerodynamics depends on the turbine speed. High TSRs imply low angle-of-attack variations, but strong wake interferences, even in the upstream phase, whereas low TSRs cause the blades to undergo big variations of their angles of attack and local speeds, eventually leading to dynamic stall.

Early models developed in the 80s and 90s were based on double or multiple streamtubes to attempt to predict the efficiency of Darrieus turbines [1, 2, 3, 4, 5, 6]. While they give a good representation of the performances observed at high TSRs, they tend to over-estimate the efficiency value at lower speeds. This has been widely confirmed by wind tunnel experiments [7, 8, 9, 10].

Following the energy crisis in 1974, the American government decided to fund a vast research program on alternative energy sources, including wind turbines. A team at the Sandia National Labs in Albuquerque, New Mexico, conducted a vast experimental study of the original Darrieus concept, both on wind tunnel models and full-scale turbines. One of their turbines reached nearly 40% efficiency, which is close to a typical large HAWT (45%) [11].

There is also various wind tunnel or water channel experimental data available, especially for high solidity/low TSRs turbines, which tend to have a lower measured efficiency (25 to 30%) [8, 10].

The present paper seeks to explore through 2D and 3D CFD simulations:

- The effect of different 2D parameters on the aerodynamic efficiency of the turbine
- Develop a better understanding of its various aerodynamic aspects
- Estimate the 3D effects
- Consider variable blade pitch control as a mean to improve power extraction.

2 Simulation method

2.1 Numerics

In the present study, the numerical simulations are performed with the commercial finite-volume code ANSYS FLUENT [12]. The simulations are conducted using the SIMPLE (Semi-Implicit Method for Pressure-Linked Equations) velocity-pressure coupling algorithm. Second order schemes are used for pressure, momentum, turbulent kinetic energy (k) and specific dissipation rate (ω) formulations. A second order implicit scheme is used for unsteady formulation when possible (cases with no variable pitch control), but is limited to first order when using a moving mesh in order to vary the instantaneous blade pitch angle. Absolute convergence criteria are set to 10^{-5} for each variable (continuity, velocity components, turbulence kinetic energy and specific dissipation rate).

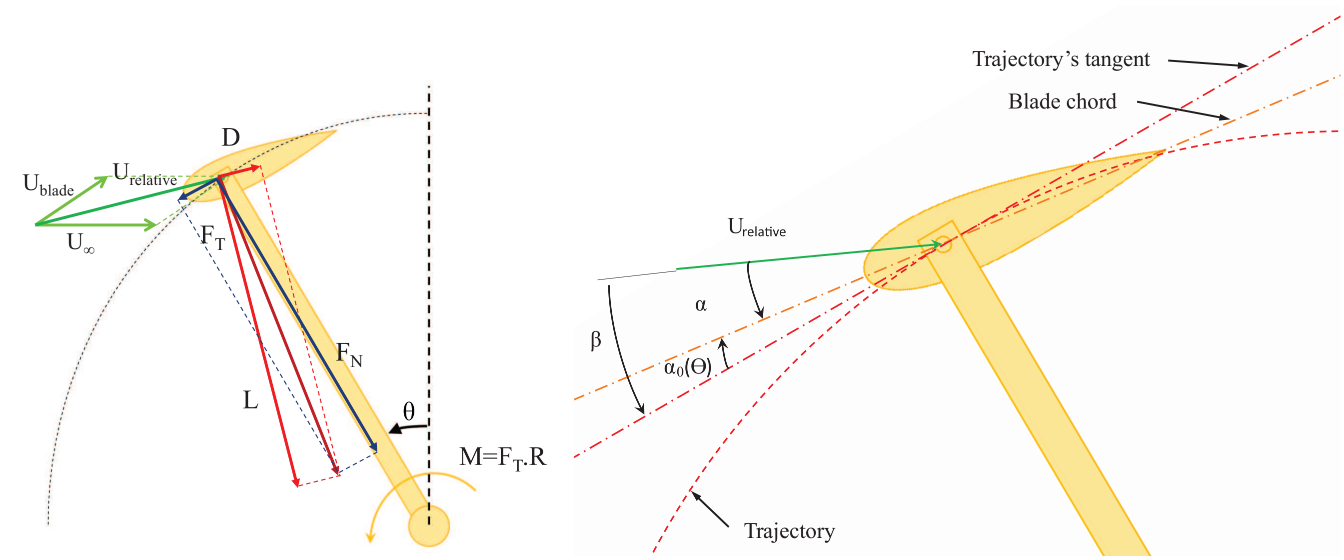

(a) *Detail of torque generation (M) from a blade in a vertical axis turbine.*

(b) *Details of the pitch angle (α_0), angle of attack (α) and force angle (β) of a turbine blade. Angles are defined counter-clockwise.*

Figure 2: *Detail of forces and various angles on a turbine blade*

2.2 Turbulence modeling

A lot of turbulence models exist, among which Spalart-Allmaras, k-ε and k-ω are the most commonly used for engineering applications. k-ω SST (*Shear Stress Transport*) is a combination of the last two: k-ω model is used near walls whereas the far field is resolved using k-ε. While k-ε uses a wall function to resolve the boundary layer, the other two models solve the Reynolds-averaged Navier Stokes equations up to the wall. This means the mesh density near the walls has to be adapted in order to be able to capture all of the viscous sublayer of the boundary layer. A commonly used criterion is the y^+ factor [1], which needs to be of order 1 for a model without wall function, and around 40 for a model with wall function (although this value depends on the wall function used).

In most cases where the boundary layer stays attached to the body, k-ε gives results similar to other models while using a coarser mesh near the walls, which reduces the time needed to complete the calculations. However, in cases with boundary layer separation and dynamic stall such as low TSRs cases, a wall function isn't appropriate to capture all the physical phenomena taking place in this important part of the flow field, and results are often off from reality [13, 14, 15].

Resolving the Navier-Stokes equations up to the walls is costly mesh-wise, but this kind of turbulence modeling has led to better agreement with experimental data, especially in oscillating airfoils and dynamic stall problems, or more generally in cases with boundary layer separation [14].

A short comparison of three turbulence models, Spalart-Allmaras with modified production term (strain-based [16, 17]), k-ω SST with low Reynolds corrections (damping of the turbulent viscosity [12]) and Transition SST has been made on the same turbine ($\sigma = 0.5486$, 3 blades, NACA0012 profile). Resulting instantaneous power coefficients for each model are shown in Figs. 4 and 5. The first comparison is made at high TSR (4.25), for which the theoretical[2] angles of attack (α) vary moderately (from $-14°$ to $14°$). The second one is made at low TSR (2.55), implying a high theoretical variation of α (from $-24°$ to $24°$) and consequently dynamic stall. As expected, the behaviour of the different models is quite similar in the high speed case, while results in the low speed example vary significantly from one model to the other.

The main factor explaining these differences is the generation of turbulent viscosity, as illustrated in Figs. 3a, 3b and 3c. The SA strain-based model generates around 10 times less turbulent viscosity than k-ω SST or Transition SST, resulting in a more chaotic flow field inside the turbine, and no statistic convergence of the instantaneous torque from cycle to cycle. It doesn't necessarily mean that the simulation is not representative of the reality, but from an engineering standpoint where

[1] y^+ is defined as $y^+ \equiv \frac{\sqrt{\tau_w/\rho}}{\nu} y$

[2] The difference between the "theoretical" angle of attack defined in Eq. 3 and the actual angle of attack of the blade is explored in section 3.1.2.

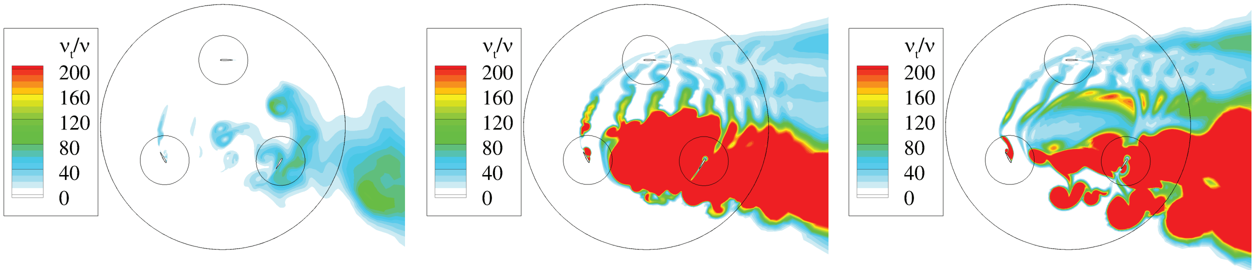

(a) *Spalart-Allmaras.* **(b)** *k-ω SST with low Reynolds correction.* **(c)** *Transition SST.*

Figure 3: *Comparison of the contours of turbulent viscosity ratio at* $\lambda = 2.55$ *for different turbulence models.*

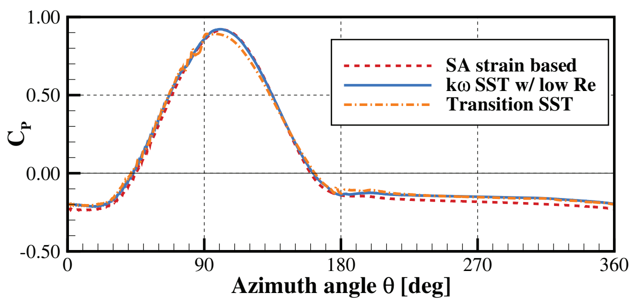

Figure 4: *Turbulence modeling behaviour at high TSR (*$\lambda = 4.25$*) for a turbine with* $\sigma = 0.5486$ *and 3 blades (*C_P *illustrated here is for one blade only), past the peak efficiency occurring at* $\lambda \approx 3.00$*, with* $Re = 2.55 \times 10^5$.

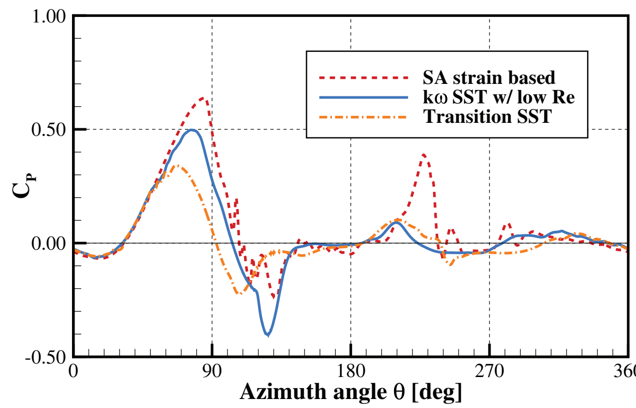

Figure 5: *Turbulence modeling behaviour of the same turbine at low TSR (*$\lambda = 2.55$*), below peak efficiency, and* $Re = 1.5 \times 10^5$.

one wants to compare a lot of different configurations and have an idea of the ideal parametric configuration, it's important to use a model that gives consistent results while being reasonably cheap to run. The simulation of a great number of turbine cycles is necessary in order to average the power output with this turbulence model. The Transition SST model gives similar results to k-ω SST in terms of cycle-averaged torque, but is less robust in some of the configurations tested. In the end, considering all its advantages in terms of dynamic stall representation and its relative low cost to run a full simulation, k-ω SST has been chosen to carry out the present parametric study.

2.3 Mesh and calculation strategy

The mesh is a critical part of a CFD simulation for engineering purposes. It has to be coarse enough so that the calculation is affordable, but also fine enough so that each important physical phenomena is captured and simulated.

The idea here is to have a mesh that can be adapted to various configurations. Mesh interfaces are used between the calculation domain and the rotating turbine, and also between the "rotor" and the smaller blade area(s). The mesh zones that include the blades are identical between all the simulations in this work, ensuring that the boundary layer behaviour is similar between the various cases. The different mesh zones used for the present simulations are illustrated in Fig. 6 while various mesh details are shown in Figs. 7a, 7b and 7c.

Unless otherwise specified (eg. low speed validation using Armstrong results [7]), the exterior domain is a square whose side is 1500 chord length. This ensures that there is negligeable blockage effect on the turbine.

Boundary conditions consist in two symmetry planes (top and bottom), a uniform pressure on the outlet boundary, and a uniform velocity on the inlet boundary with magnitude U_∞. Turbulent conditions at the inlet boundary are 0.1%

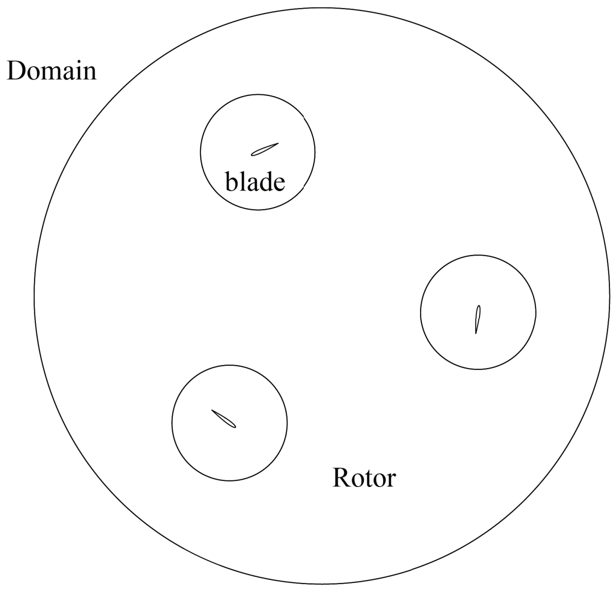

Figure 6: *Identification of the different mesh zones. Computation domain extends over* $750c$ *in all directions.*

turbulent intensity and $0.001c$ turbulent length scale, yielding $\frac{\nu_t}{\nu} \approx 0.05$.

A y^+ value of order 1 is sought at the blades. The worst case scenario (high TSR hence high Reynolds number and thin boundary layers) was used to determine the boundary layer thickness and thus the required cell's scaling. This implies that y^+ is around 1 in high TSRs cases ($\lambda = 7$ and above) and smaller than 1 in lower speed cases.

The number of nodes on each blade is 360, but low TSR results have showned that it was not enough in deep-stall cases, probably due to difficulties in the prediction of the boundary layer transition position and in the resolution of the separation bubble. Finer meshes were tested in such conditions, with a lot more points (up to 700) on the blades and finer boundary layer meshes, but no rigorous mesh-independence was obtained as was the case for larger TSRs.

A 3D mesh is created based on an extrusion of the 2D mesh. Half the blade span is meshed in 3D and a symmetry boundary condition is imposed on the mid-plane. The spanwise discretization is uniform in the central part of the blade, close to the symmetry plane, while the last $0.5c$ length from the wingtip is refined. A first mesh was tested with 13 spanwise nodes per chord length on the central part, and a refinement close to the tip/end-plate with a y^+ value of 2. A second, coarser mesh, was tested with 7 spanwise nodes per chord length in the central part and $y^+ = 7$ at the wing tip, and showed no noticeable differences in the results along the cycle.

Time step is expressed on a per cycle basis. A quick comparison showed that around 1000 time steps per cycle were sufficient in most cases, but some particular ones needed up to 5000 to reach result independence. For this reason, this conservative value is used in 2D simulations in order to avoid undesired effects on the flow field. For the 3D experiments (focused on high efficiency cases, with tip speed ratios higher than the optimum value, hence no massive stall on the blades), we use the 1000 time steps per cycle value after verifying the results convergence with a 2500 time step per cycle simulation. Other research groups used much coarser time steps (around 360 time steps per cycle) [15], but our calculations showed that at such low values, result independence is not achieved with the present modeling approach.

A minimum number of rotations is necessary to ensure that a repeatable power extraction cycle is achieved, but this number is case-dependant and must be estimated for each simulation by comparing the C_P cycle to the previous ones. For example, high speed, unstalled case ($\lambda = 6.38$), of a low solidity ($\sigma = 0.1819$) three-blade turbine needs around 10 complete turbine cycles to reach cycle-averaged torque convergence. Other low speed cases, need in excess of 20 turbine rotations to reach it. In all simulations presented here, cycle-averaged convergence was reached before accumulating data and statistics.

2.4 Model validation

2.4.1 High TSR, low solidity

High tip speed ratios ($\lambda = 4$ to 6) are the least challenging cases to simulate because the blades never actually reach too large angles of attack, hence never encounter stall. Since k-ω SST was developed for aeronautic applications, the results are expected to be satisfactory. However, good and reliable data on test turbines operating in this range of TSR is rare. The solidity needs to be low (σ from 0.1 to 0.2) to have a performance peak around $\lambda = 5$. This means high ratio of turbine radius to blade chord. The best example of such a turbine is the 5m Sandia test turbine [18], which has 3 blades and mid-height solidity of $\sigma = 0.1829$, but has the shape of the original Darrieus, i.e. the "egg-beater" shape.

It has been shown that around the peak efficiency, most of the power is extracted in the central, almost straight-blade, area.

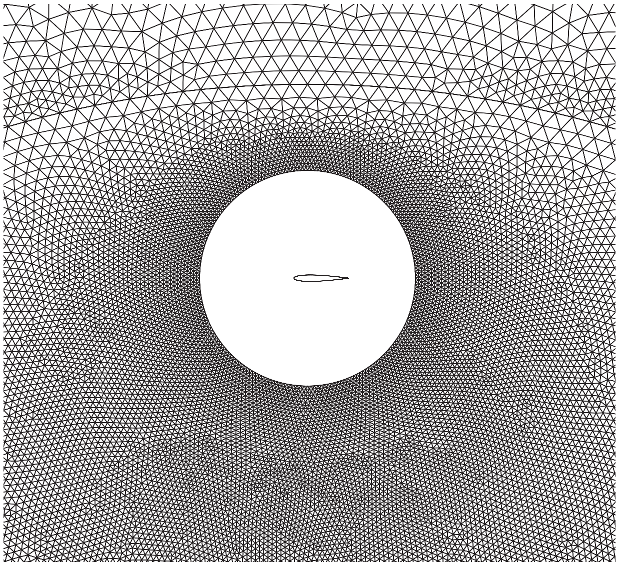

(a) *Detail of the mesh of the rotor around a smaller area interface. Part of the domain mesh is visible on the top part of the figure.*

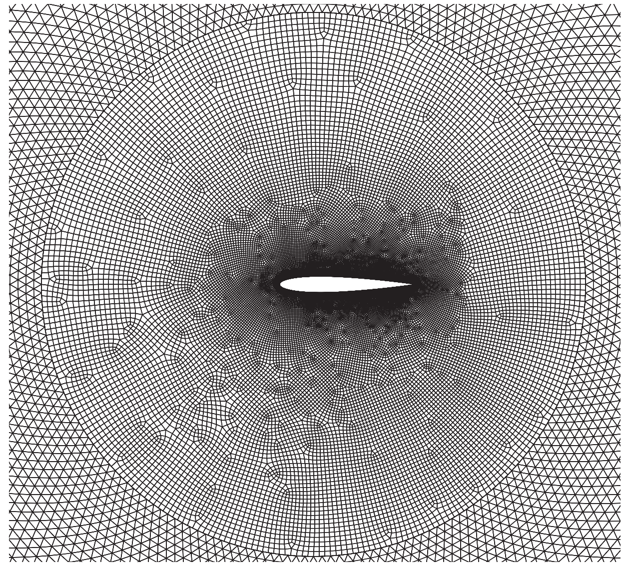

(b) *Detail of the mesh of the small area around a blade.*

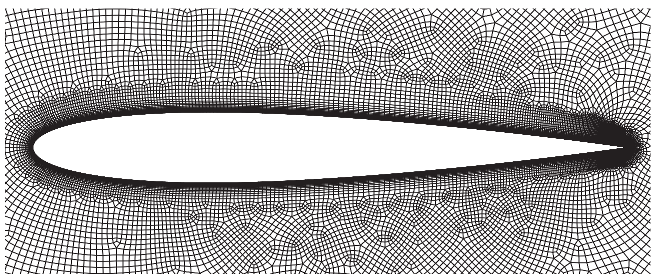

(c) *Detail of the boundary layer mesh of a blade.*

Figure 7: *Various details of the mesh.*

In fact, most of original Darrieus turbines used three-part blades, with only the center, high local radius part, being profiled, the extremities only serving the role of connecting arms. The Sandia 5m turbine, however, used fully profiled blades. Because of that, a 2D simulation should give good results around the peak efficiency. At lower speeds, the power extraction is more evenly distributed along the turbine, with upper and lower parts of the turbine having higher local solidities, hence being more efficient at these TSRs.

Results are presented in Fig. 8. As expected, the optimal tip speed ratio is relatively well represented. However, at lowers TSRs, the efficiency predicted by the 2D numerical simulation drops faster than the experimental data, due to the “egg-beater” shape of the turbine. The gap between experiments and 2D simulations is primarily the result of 3D effects, and a 20% drop, as measured here around the peak, is not inconsiderate.

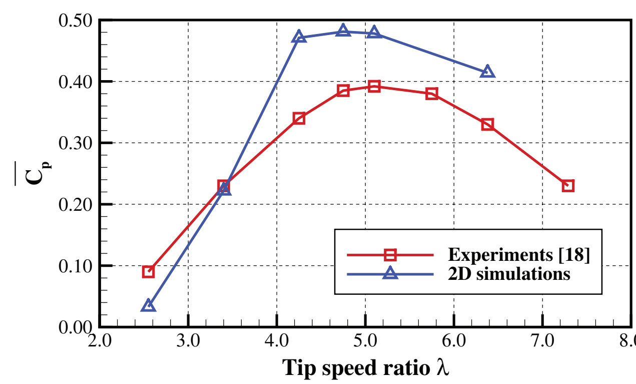

Figure 8: *Comparison of the experimental results for the Sandia 5m turbine, and 2D simulations of a three-blade,* $\sigma = 0.1829$ *turbine.*

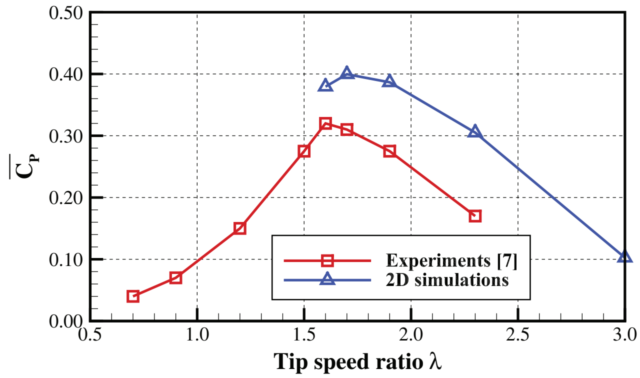

Figure 9: *Comparison of the experimental results and 2D simulations of a three-blade turbine, in the* $-6°$ *fixed pitch configuration with* $\sigma = 0.915$.

2.4.2 Low TSR, high solidity

Low tip speed ratios ($\lambda = 1$ to 3) are far more difficult to simulate because of the high instantaneous angles of attack reached by the blades (see Eq. 3 and Fig. 11), combined with highly varying relative speeds. This leads to boundary layer separation and dynamic stall for such cases.

Turbines operating in this range of TSR have higher solidity (typically around 0.5), either by an increased number of blades or a reduced turbine radius. Examples of such turbines are more common in the literature as they are easier to manufacture and fit more easily in a wind tunnel or a water channel.

In this article, the simulations are compared to wind tunnel experiments by Armstrong and al. [7], whose straight-blades turbine has a solidity $\sigma = 0.915$ and a peak efficiency $\overline{C_P} = 0.27$ at $\lambda = 1.6$ and $Re = 5.0 \times 10^5$. It was tested at the University of Waterloo Live Fire Research Facility, whose dimensions and characteristics are described by Devaud and al. [19]. The domain size and boundary conditions have been modified for this particular case to match the experimental rig, albeit only in 2D.

They also provided results with various pitch angles ($3°$, $0°$, $-3°$, $-6°$, $-9°$ and $-12°$) that can be used to further validate the model, with $-6°$ being the optimal configuration in this case.

Results of the simulations are presented in Fig. 9. Again, conditions for peak efficiency are well predicted despite the overestimation of the 2D simulations. Low TSRs, before the optimal value of $\lambda = 1.6$ were not simulated here, except for the $\lambda = 0.70$ case, which gave a cycle-averaged efficiency $\overline{C_P} = 0.02$, lower than what is observed on the test turbine. Low speed simulations of other configurations of this turbine (with no pitch angle) showed the same behaviour as in the Sandia 5m simulation, with the experimental curve being higher than the simulation one.

Further discussion on the effect of the pitch angle is presented in the next section. The important thing to note here is that the model has a good behaviour past the optimal TSR, with an almost constant relative gap between the 2D simulation and 3D experimental results. This difference is mainly due to the various 3D effects encountered in the turbine, but also due to the particular shape of the "wind tunnel" used, with a ceiling high above the testing plane, and ground proximity.

2.5 Modeling limitations

Deep wing stall is always a challenge in CFD, so it's not such a surprise that the simulations give poor matching of experimental data in theses cases, with lower efficiencies than what is observed in real turbines. On the other hand, they tend to give quite good estimations of the TSR where peak efficiency is obtained, and higher TSRs behaviour is in accordance with the experimental results.

The gap between 2D simulations and real, 3D turbines is the result of 3D effects [10]. It depends on several factors, including the turbine shape and its surroundings, so it's not easy to extrapolate an efficiency value for a particular real turbine based solely on 2D results. However, the qualitative impact of varying 2D parameters should be maintained in 3D.

3 RESULTS AND DISCUSSION

3.1 Flow topology across the turbine

The power-extraction performance of each blade within a VAT is strongly linked to the effective flow conditions seen by the rotating blades. These effective conditions are characterized by the instantaneous effective velocity (magnitude and direction) and the angle of attack. A good understanding of the actual flow around each blade is important when seeking methods to improve the global efficiency through the control of instantaneous blade angle.

3.1.1 Velocity magnitude and direction

The easiest assumption that can be made about the flow field across a VAT is to consider it uniform and equal to U_∞. This assumption may however be too simplistic. Indeed, a turbine blade makes 2 passes in the same streamtube every rotation. In the first one, it extracts energy, thus reducing the kinetic energy available downstream, by reducing the velocity magnitude. This is represented in Fig. 10.

This reduction in velocity, associated with the the extraction of energy, also implies that the streamtube expands while flowing through the turbine. This creates transverse velocities, also affecting the angles of attack, even in the upstream phase.

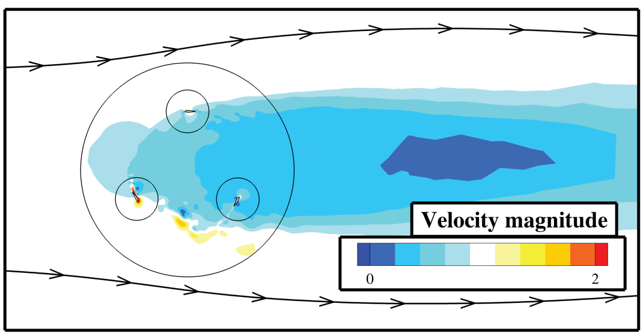

Figure 10: *Velocity magnitude contours and streamtube for a three-blade turbine with* $\sigma = 0.5486$ *and* $\lambda = 2.75$.

Another important point is that the speed reduction is not symmetrical. A drop in velocity magnitude is only observed where the blade actually extracts energy, meaning that when it stalls, no drop in magnitude is noticeable downstream. If the TSR increases, the angles of attack drop, reducing stall, while the average relative velocity increases. It means that the turbine extracts more power during the first pass, eventually creating a low speed area about the size of the turbine if no stall is observed. This decrease in available energy lowers the lift forces on the second pass, but also decreases the drag.

In the end, the best configurations are often those that extract most energy on the first 180° of the cycle (see the difference between Figs. 4 and 5 for example), with the second part creating considerably lower efforts on the blades due to the low local speeds and angles of attack.

3.1.2 Angle of attack: theory vs. simulations

The instantaneous angle of attack can be calculated with Eq. 3, under the assumption of a uniform free stream velocity in the axial direction:

$$\alpha[rad] = \arctan\left(\frac{1}{\lambda \cdot \sin(\theta)} + \frac{1}{\tan(\theta)}\right) + \theta - \frac{\pi}{2} \quad . \qquad (3)$$

An example of instantaneous angles of attack for different TSRs is given in Fig. 11, which shows that the blades of a turbine operating at low speeds encounter much higher angles of attack than a turbine operating at high speeds. In the $\lambda = 5.10$ case, the theoretical angle of attack is never higher than the static stall angle for the profiles tested here ($\alpha_{stall} \approx 13°$).

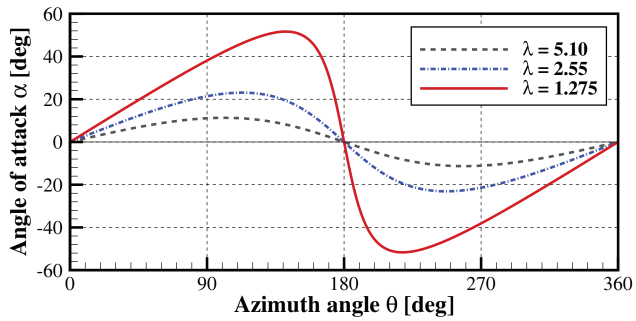

Figure 11: *Theoretical instantaneous angle of attack in a Darrieus turbine for different tip speed ratios* (λ).

In cases where the turbine extracts significant power from the flow, it should be more accurate to use a reduced flow speed for the return part of the cycle, for example $0.5 \times U_\infty$. This would actually divide the angle of attack by 2 in the downstream part of the cycle, as shown by the theory curve of Fig. 12. This correcting factor would depend of course on the amount of power extracted in the first, upstream pass.

Even though the angle of attack is literally defined as the angle between the airfoil chord and the flow direction far from the foil, it is possible to extract a “local” angle of attack from the CFD data, by considering the average flow direction and magnitude along the blade path at a virtual point located two chord length ahead of the blade on its trajectory. This method gives a good estimate of what the real effective angle of attack of the blade is as shown in Fig. 12 which corresponds to a low-speed case where stall and boundary layer separation occur. Significant differences between theory and simulations in the 180° to 240° range are thus expected, and are due to the turbulence and the surplus in kinetic energy available (creating more drag) linked to the stalling blade in the upstream phase.

The other difference between theory and simulation in Fig. 12 is the more or less constant gap in the upstream part of the cycle. This is due to the blockage effect from the turbine, that affects the flow upstream of it. The speed seen by the blade is not exactly U_∞, but a slightly lower speed with a slight angle, as part of the flow tries to go around the turbine and not through it. More energy extracted means greater blockage.

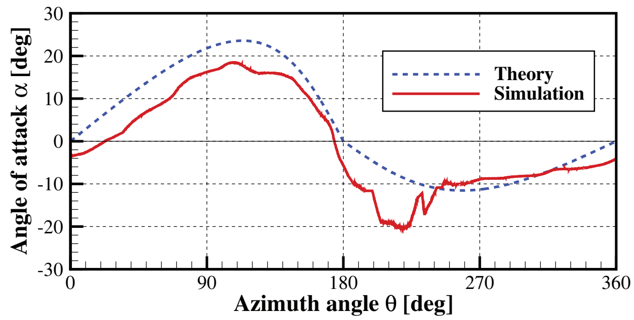

Figure 12: *Comparison between corrected theoretical angle of attack (flow speed divided by 2 in the downstream part), and measured angle of attack from CFD simulation. Tip speed ratio is* $\lambda = 2.5$ *with a three-blade* $\sigma = 0.5486$ *turbine.*

3.2 2D parametric study

3.2.1 Effect of solidity

Earlier models based on multiple streamtubes were used in the 80s to make a global parametric study, especially on the effect of solidity σ. Results from these models are shown in Fig. 13. These models predict $\overline{C_P}_{max} \geq 0.4$ even for high solidity turbines ($\sigma \approx 0.5$). However, such a performance has not been achieved experimentally for turbines with such solidities [8, 9, 10, 20].

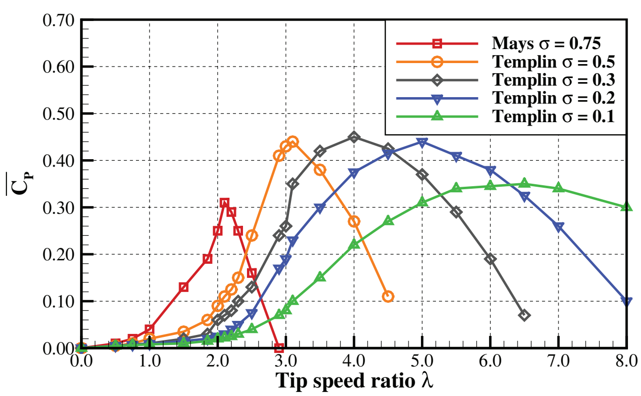

Figure 13: *Predictions of efficiency for different solidities* σ *using multiple streamtubes models [1, 3], extracted from [21].*

Figure 14 compares the results of 2D simulations of three-blade turbines with various solidities. The main difference with older models appears in the lower TSR region, where angles of attack are large enough to cause dynamic stall, which reduces power extraction. The maximum efficiency decreases when solidity increases, which is in accordance with experimental observations. Those are 2D results which implies that

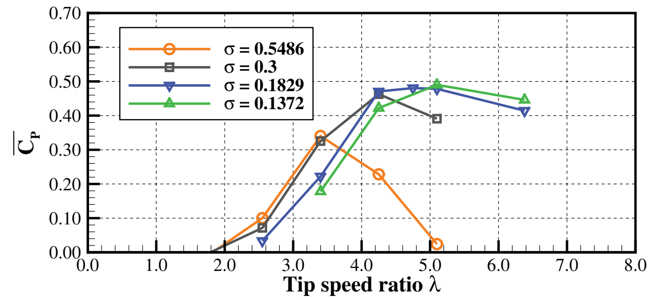

Figure 14: *Present CFD simulation of three-blade turbines with different solidities* σ*.*

actual quantitative values are expected to be less in 3D. 3D simulations are needed to evaluate this impact.

3.2.2 Effect of the number of blades

The number of blades has an effect on the global torque. More blades leads to a smoother torque on the shaft (less fluctuations). However, increasing the number of blades means increasing the number of connecting shafts, hence increasing the turbine drag. It also implies that for the same radius and blade chord, the solidity is increased dramatically, which can be detrimental in terms of maximum efficiency. Figure 15 shows the effect of the number of blades but for a case where solidity is maintained constant with the number of blades changing. For comparison, an extra case where $\frac{R}{c}$ is kept the same is also included. Note that in this study, the drag of possible connecting arms is not taken into account.

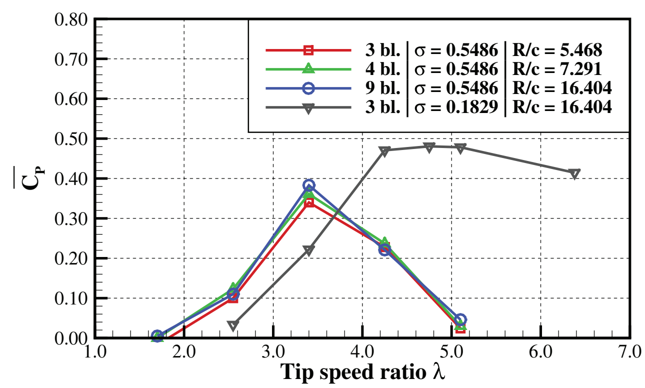

Figure 15: *Effect of the number of blades in turbines with the same solidity* $\sigma = 0.5486$ *or the same* $\frac{R}{c} = 16.404$*.*

As expected, increasing the number of blades while keeping the solidity constant does not change significantly the maximum efficiency. On the other hand, for a turbine with a fixed radius, it seems preferable to reduce the number of blades in order to decrease the solidity to achieve better efficiency, although at higher speeds. This is however only valid within a reasonable solidity range. Indeed, a too low solidity would decrease the maximum efficiency, because each blade wake would not be convected fast enough for the next one to have a clean stream. This reduces the effective angle of attack to the point that no large lift forces are created.

Optimal solidity value, without any alteration to the design (e.g., pitch angle), seems to be around $\sigma \approx 0.2$.

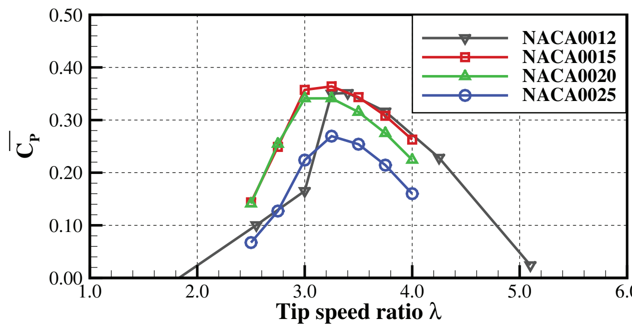

Figure 16: *Effect of the thickness of the blade profile in a three-blade turbine with solidity* $\sigma = 0.5486$.

3.2.3 Effect of blade thickness

Different symmetrical NACA profiles have been tested in a three-blade, $\sigma = 0.5486$ configuration: NACA0012, NACA0015, NACA0020 and NACA0025. Results are shown in Fig. 16.

We see that increasing the blade thickness tends to enlarge the range of TSR where the turbine extracts energy with good efficiency. Increasing it too much, however, and the added drag becomes too important and $\overline{C_P}$ values reached starts to plummet.

In this case, NACA0015 is optimal compared to thinner and thicker profiles. Comparing instantaneous power coefficient at a particularly sensitive TSR ($\lambda = 3$, close to the speed of peak efficiency) for one of the three blades helps understand the differences between each of these cases (Fig. 17).

On the first part of the cycle, before 90°, NACA0012 is slightly better than the other thicknesses, due to its lower drag. However, it stalls around 100° while the thicker profiles don't, allowing them to reach a higher mean $\overline{C_P}$ value overall.

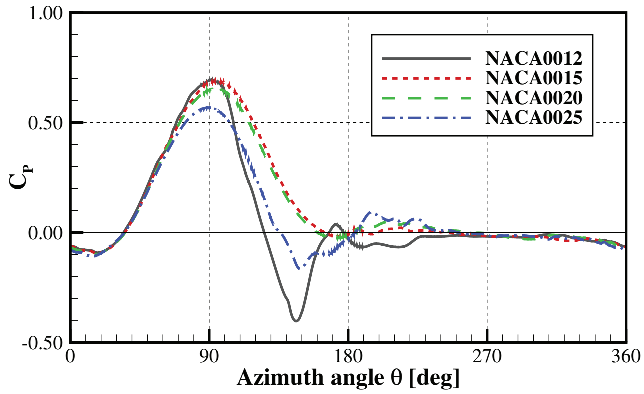

Figure 17: *Instantaneous power coefficient from 1 blade in a three-blade turbine with solidity* $\sigma = 0.5486$ *at* $\lambda = 3.00$.

	$\lambda = 3.40$		$\lambda = 5.10$	
Re	2×10^5	1×10^6	3×10^5	1.5×10^6
$\overline{C_P}$	0.158	0.474	0.454	0.508
Rel. diff.	66.7%		10.6%	

Table 1: *Numerical comparison of the effect of Reynolds number at low and high TSR.*

3.2.4 Effect of Reynolds number

The Reynolds number, especially around 10^5, has a significant effect on the aerodynamics of a wing. Larger values help delay stall and lower the drag thanks to the boundary layer being more resistant to separation. It also allows slightly higher lift coefficients while reducing slightly the drag coefficient due to the slender effective bodies.

On the simulation point of view, the only difference is that the boundary layer is thiner in a high Reynolds case than it is in a low Reynolds one, so the mesh close to the blade has to be adapted in order to keep the y^+ value below 1. This leads to larger meshes, hence longer calculations. Single-blade turbine have thus been used here in order to keep the calculation cost low for this particular analysis.

Simulations of a single-blade, $\sigma = 0.1829$ turbine have been carried out with two different Reynolds numbers. The high-Reynolds turbine operates at $Re = 1.5 \times 10^6$ and $\lambda = 5.10$, while the low-Reynolds turbine operates at $Re = 3 \times 10^5$ and $\lambda = 5.10$, the same as the Sandia turbine. Other simulations of the same turbines have been run at a lower TSR, $\lambda = 3.4$, in order to evaluate the effect of increasing the Reynolds number in stalled cases. Results are summarized in Table 1, and the instantaneous power coefficients are compared in Fig. 18.

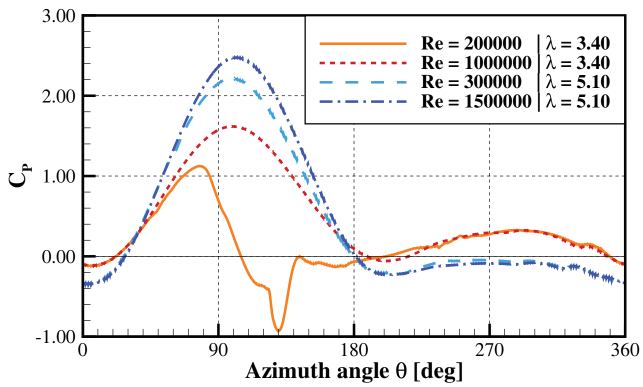

Figure 18: *Comparison of instantaneous power coefficient of a single-blade turbine with solidity* $\sigma = 0.1829$ *at* $\lambda = 3.40$ *and* $\lambda = 5.10$*, for various Reynolds numbers.*

At $\lambda = 5.10$, close to the peak efficiency, the difference between low Reynolds and high Reynolds numbers appears only in the upstream phase, where the power coefficient of the high-Re case reaches a slightly higher value, due to the higher lift and lower drag. There's almost no differences in the downstream phase, where the effective local Reynolds numbers are lower and relatively closer between the two simulations.

At $\lambda = 3.40$, differences are much more important, mainly due to the fact that for the high-Reynolds case, the blade does not stall, while it does in the low-Reynolds case.

Previous studies, e.g., [7], suggest that there is a Reynolds number independence over $Re = 5 \times 10^5$ in the case of Darrieus turbines. In most practical applications, the Reynolds number would typically be higher than this value.

3.3 3D effects

In this part of the study, a simple single-blade NACA0015 turbine has been used, with blade aspect ratios of $AR = \frac{H}{c} = 7$ and $AR = 15$. Two different end-plates have also been tested in the $AR = 7$ case. The turbine solidity is $\sigma = 0.2857$, and simulations are carried out at $\lambda = 4.25$ and $Re = 2.5 \times 10^5$, slightly past the maximum efficiency tip speed ratio, in order to avoid massive stall that would require a much finer mesh and time step size, as discussed in section 2.3. All those results are compared below to their 2D equivalents.

3.3.1 Blade aspect ratio effect

Table 2 and Fig. 19 show the results obtained for the two blade aspect ratios tested.

Turbine	$\overline{C_P}$	3D/2D efficiencies ratio
2D	37.8%	–
$AR = 7$	15.8%	41.8%
$AR = 15$	26.1%	69.0%

Table 2: *Numerical comparison between the performance of 3D turbines with different blade aspect ratios, and the 2D results.*

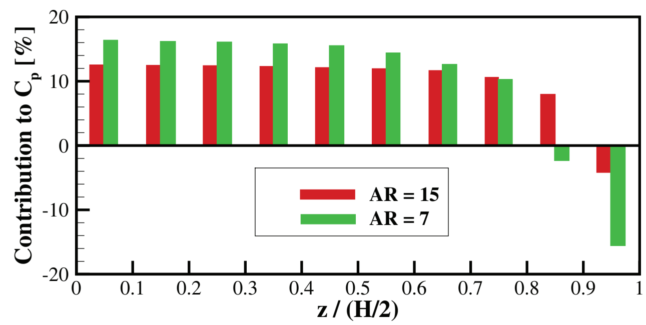

Figure 19: *Comparison of the local contribution to* $\overline{C_P}$ *along the half-blade span for the* $AR = 7$ *and* $AR = 15$ *cases.*

Previous experimental studies [10] showed that a turbine performance is heavily linked to its blades aspect ratio, with 95% of the 2D efficiency value obtained with $AR > 72$. As modeling such turbines requires a very large mesh and would thus be too computationally expensive, the present comparisons have been made with lower blade aspect ratios.

As expected, the drop is massive with the $AR = 7$ case, where only 41.8% of the 2D efficiency is reached. Doubling the aspect ratio gives a significant boost in efficiency, reaching nearly 70% of the ideal 2D case. This tendency is in agreement with Li and al. results [10].

The effect of lengthening the blade is illustrated in Fig. 19 from the contribution of each 10^{th} of a half-blade span to total $\overline{C_P}$. The contribution of each blade section is more uniform in the case of the longer blade (a perfect distribution would be 10% for each 10^{th} of the half-blade span), meaning that the flow has a more 2D behaviour when using a longer blade. As expected, the presence of the blade tip is relatively less detrimental with a longer blade.

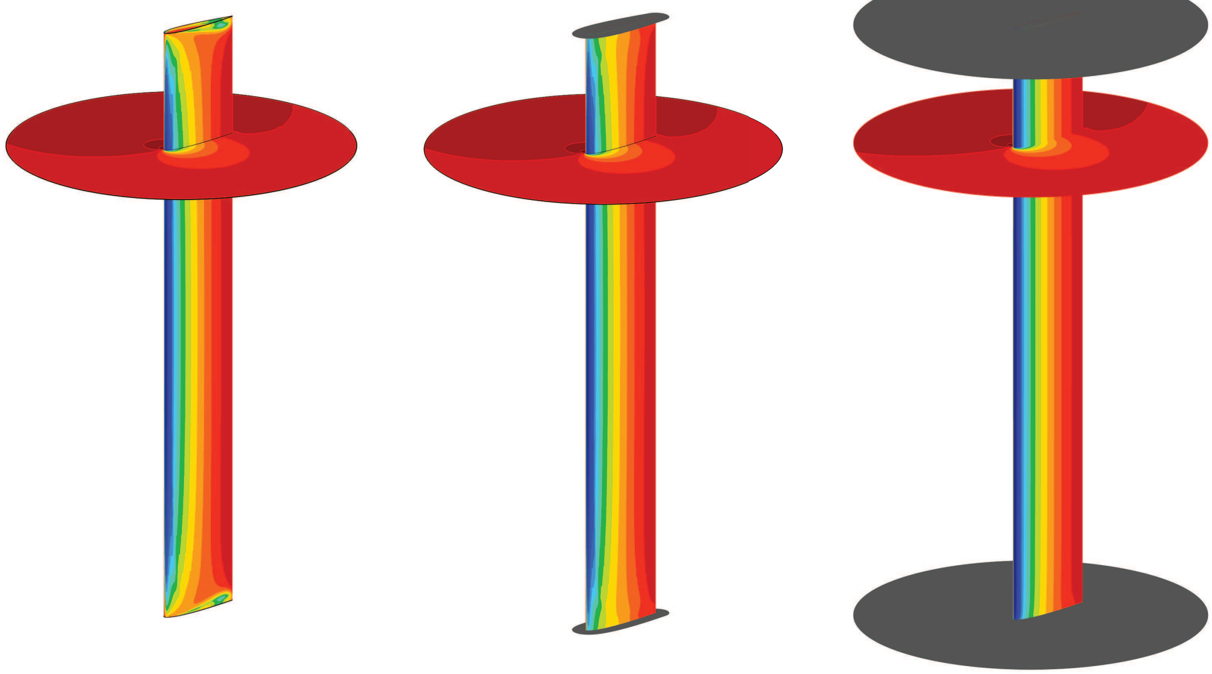

(a) *$AR = 7$ with no end-plate.* **(b)** *$AR = 7$ with "NACA" end-plate.* **(c)** *$AR = 7$ with circular end-plate.*

Figure 20: *Contours of pressure on the blade at $\theta = 108^\circ$, close to the peak instantaneous C_P, for the three $AR = 7$ configurations.*

Turbine	Total $\overline{C_P}$	3D/2D eff. ratio	End-plate $\overline{C_P}$ cost
2D	37.8%	–	–
$AR = 7$ no end-plate	15.8%	41.8%	–
$AR = 7$ circ. end-plate	−10.5%	–	40.9%
$AR = 7$ "NACA" end-plate	18.8%	49.7%	1.7%

Table 3: *Numerical comparison between the performance of 3D turbines with different end-plates, and the 2D results.*

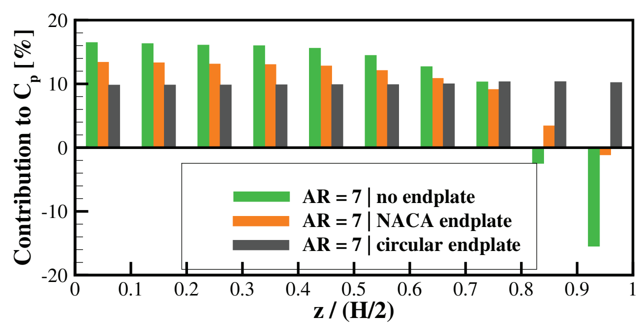

Figure 21: *Comparison of the local contribution to $\overline{C_P}$ along the half-blade span for the $AR = 7$ case with and without end-plates.*

3.3.2 End-plates effect

Two end-plates have been simulated in order to evaluate the gain in performance made possible by preventing formation of blade-tip vortices. Figures 20a, 20b and 20c show the various configurations tested.

The first one consists in a circular flat plate with no thickness, covering the whole blade mesh area (diameter$= 4c$). The second one is a $0.15c$ extension of the blade profile which we refer to as the "NACA" end-plate. Figure 21 and Table 3 compare these results with those of the 2D and the no-end-plate simulations.

The simulation with the large circular end-plate is interesting in two aspects. The first one is that it shows that it is possible to have an almost constant load distribution on the blade, closer to the 2D optimum case. The second point is that the Darrieus turbine is very sensitive to drag, and the benefit of uniform loading is completely annihilated by the energy loss associated to the drag of this large flat plate.

The NACA end-plate offers slightly less effective uniformization, but it offers a 10% efficiency boost compared to the case with no end-plate, which is quite interesting for such a small end-plate. Most of the improvement is made in the region close to the blade tip. It shows that a small end-plate device can be quite useful in situations where the blade aspect ratio is limited, but the design/size of this end-plate is critical, and a badly sized one may cost a lot more energy than the gain it offers.

3.4 Pitch angle analysis

3.4.1 Effect of fixed pitch angle

Various experiments showed that, at least for high solidity cases, changing the pitch angle from $\alpha_0 = 0°$ to a small toe-out angle increased the efficiency of the turbine [7, 9]. Simulations with non-zero pitch angle α_0 (see Fig. 2b) have been performed for a three-blade turbine with $\sigma = 0.5486$, and global results are shown in Fig. 22.

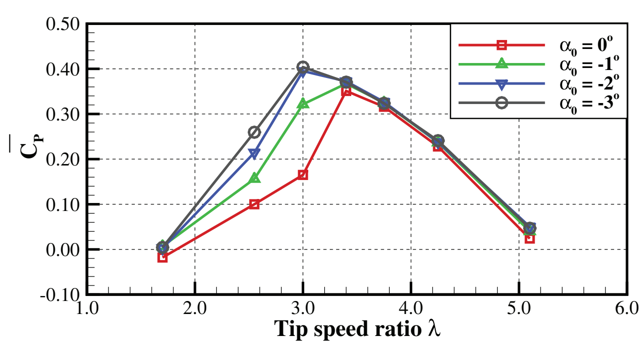

Figure 22: *Effect of the pitch angle* α_0 *on the efficiency of a three-blade turbine with solidity* $\sigma = 0.5486$.

The case at $\lambda = 3.00$ is the best example to help understand in which way setting a small toe-out angle improves the efficiency of the turbine. A comparison of the corresponding instantaneous power coefficients is presented in Fig. 23.

Setting a small amount of toe-out to the blade has the effect of reducing the angle of attack in the upstream phase, and increasing it in the downstream one. Both these effects are good for a Darrieus turbine, as the angles of attack are too high in the first pass due to the free stream velocity, and too low (in negative values) in the second one due to the velocity deficit.

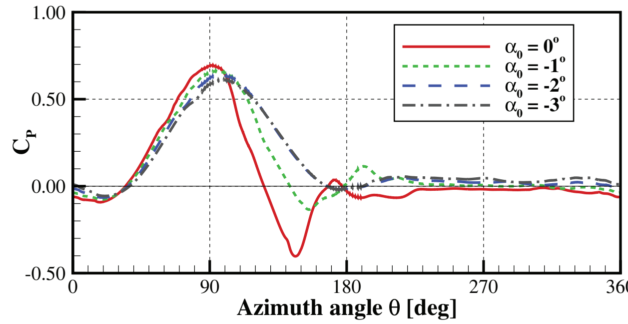

Figure 23: *Instantaneous power coefficient of one blade of a three-blade turbine with solidity* $\sigma = 0.5486$ *at* $\lambda = 3.00$*, for various pitch angle values.*

It is clearly visible on Fig. 23 that increasing the negative pitch angle delays power extraction as the actual angle of attack is lower. It also permits to avoid the stall that is present in the $\alpha_0 = 0°$ and $\alpha_0 = -1°$ cases. Finally, the power extracted in the downstream phase is slightly higher with the largest negative pitch angle $\alpha_0 = -3°$, because this turbine extracts a little bit less energy in the upstream phase.

3.4.2 Investigating variable pitch functions

Some previous studies have used genetic algorithms to attempt to determine an optimal pitch control function [20]. In the present study, we propose to control the pitch angle of the blades along their cycles in order to ensure an almost constant angle of attack during the whole cycle. One can observe that the force angle switches from positive to negative in the downstream phase of the blades, which implies that the angle of attack has to be negative in this part of the cycle in order to have the lift in the correct direction. A difficulty encountered is that our pitch function is based on the theoretical angle of attack, defined in Eq. 3. Results from section 3.1.2 showed that this approximation is good in the upwind phase, but not that much in the downstream phase.

The variable blade pitch function used here is thus defined in parts depending on the position of the blade in its cycle. Away from the $\theta = 0°$ and $\theta = 180°$ azimuth angles, the function is simply the opposite of Eq. 3 with an adjustable offset α_{cst} (*target* angle of attack), as shown below:

$$\alpha_0(\theta) = \begin{cases} \text{if } 22.5° < \theta < 157.5° \\ -\arctan\left(\frac{1}{\lambda \cdot \sin(\theta)} + \frac{1}{\tan(\theta)}\right) - \theta + \frac{\pi}{2} + \alpha_{cst} \\ \text{if } 202.5° < \theta < 337.5° \\ -\arctan\left(\frac{1}{\lambda \cdot \sin(\theta)} + \frac{1}{\tan(\theta)}\right) - \theta + \frac{\pi}{2} - \alpha_{cst} \end{cases} \tag{4}$$

Other parts of the cycle are third degree polynoms, whose goal is to join the two opposite "positive" and "negative" parts, while ensuring smooth continuity in terms of the angle of the blade, as well as reasonably moderate rotational motion of the blade. This is done to avoid shedding of vorticity when switching from the constant angle of attack region to the "buffer" region. Figure 24 shows the function applied for different target angles of attack with a 45 degrees buffer zone around $\theta = 0°$ and $\theta = 180°$.

The energy cost associated to this pitch control is computed from the product of the instantaneous torque at each blade axis with its pitch angular velocity. Efficiencies are reported below including or not this energy cost.

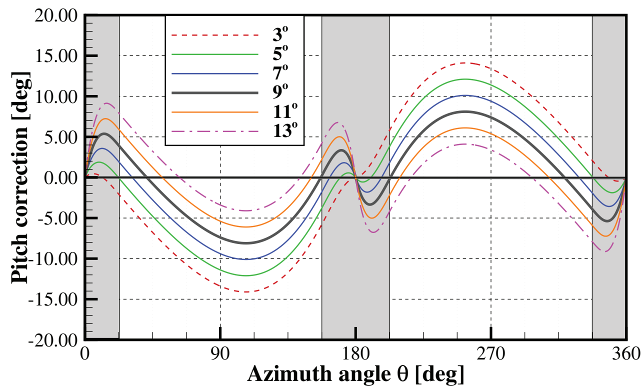

Figure 24: *Pitch angle correction for different target α_{cst}. Grey areas are the buffer zones.*

Table 4 and Fig. 25 shows the results obtained at $\lambda = 3.4$ for a $\sigma = 0.5486$ three-blade turbine, and various target angles of attack.

Target α	$\overline{C_P}$ wo/ cost corr.	$\overline{C_P}$ w/ cost corr.	Rel. diff. with no pitch control
3°	28.39%	25.49%	−42.4%
5°	44.79%	41.99%	−5.1%
7°	56.08%	53.00%	+19.7%
9°	60.04%	56.29%	+27.1%
11°	60.97%	56.19%	+26.9%
13°	59.86%	53.72%	+21.3%

Table 4: *Numerical comparison of the different variable pitch angle functions compared to the original, fixed-blade-pitch turbine.*

Based on the overall efficiency, the optimum target angle of attack is around 9°, close to the maximum lift-to-drag ratio of the profile. The improvement is made not only on the first part of the cycle, with a slightly higher peak value and a much broader extraction peak, but also on the downstream phase, where the loss of energy is lower with high angle of attack target values.

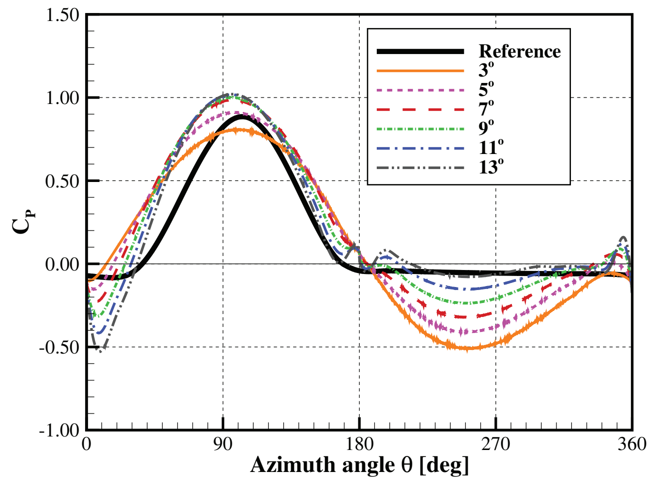

Figure 25: *Instantaneous power coefficient of one blade of a pitch-controlled three-blade turbine with solidity $\sigma = 0.5486$ at $\lambda = 3.40$ for different target angles of attack, compared to the reference simulation without pitch control.*

One can also note that these 2D values come really close to the Betz limit[3] for the optimum cases. Even considering a relative reduction of about 20% for 3D effects, these results are quite encouraging and quite competitive with other turbines technologies.

Further simulations have been performed keeping the optimum $\alpha_{cst} = 9°$ target value in the upstream phase, but targeting different α in the downstream phase. The effect of doubling or halving the AoA in the downstream phase is presented in Fig. 26 and in Table 5.

Downstr. α	$\overline{C_p}$ wo/ cost corr.	$\overline{C_p}$. w/ cost corr.	Rel. diff. with no pitch contr.
−9°	60.04%	56.29%	+27.1%
−4.5°	55.49%	52.87%	+19.4%
−18°	54.08%	49.72%	+12.3%

Table 5: *Numerical comparison of the different downstream angles of attack compared to the original, fixed-blade-pitch, turbine.*

[3] 59.3% considering a single extraction plane, 60.4% considering 2 consecutive extraction planes.

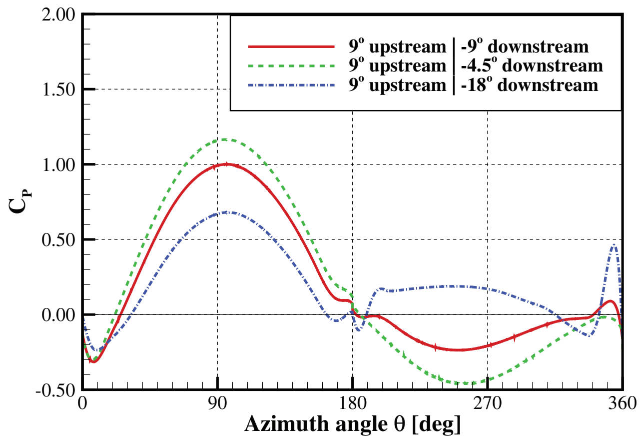

Figure 26: *Instantaneous power coefficient of one blade of a three-blade turbine with solidity* $\sigma = 0.5486$ *at* $\lambda = 3.40$*, for different targeted angles of attack in the downstream phase.*

The most interesting observation here is an apparent coupling between the upstream and downstream phases, meaning that the more energy extracted on the first phase, the higher the energy cost in the downstream phase. Because of this, setting the theoretical downstream angle of attack to -18° and -4.5° does not change much the uncorrected efficiency value. The only difference in efficiency between these two cases is the higher cost to impose a -18° angle of attack compared to -4.5°.

Moreover, despite being slightly less efficient than the "base" case with 9° target angle of attack, the case with a doubled angle of attack in the downstream phase shows a lot less variations in the overall torque of the turbine thanks to its more balanced distribution (considering the contributions of all three blades) between upwind and downwind extraction. This is quite interesting for real world applications where reducing torque ripple helps reducing fatigue failure of the mechanical components.

4 Conclusions

Summarizing the present results, it seems always best to have a solidity around 0.2, implying turbines with large $\frac{R}{c}$. Most real-size Darrieus turbines in the 70s had 2 blades, which seems to produce the best efficiency. However, torque ripple in such turbines was so important that their mechanical components always failed in the long term, a drawback compared to their HAWT counterparts.

Nowadays, prototypes with three-blade (or more) are more common. They have much less torque ripple but increased solidity that reduces their maximum efficiency.

Simulation results for fixed, non-zero, pitch angle cases show that there is a great potential of improvement in "medium" tip speed ratios (2 to 4) for turbines with solidity around 0.5. This opens the way to dynamic pitch control, with the ability to maximize blade lift to drag ratio over a complete cycle.

This study also gives a more precise look on what is happening in the turbine, and what parameters have the most influence. The parametric study showed that most efficient fixed pitch cases are those with solidity around $\sigma = 0.2$, which is consistent with the experimental data available. Such turbines exhibit a larger radius-to-chord ratio, around 15 for a three-blade turbine.

Higher solidity turbines can't reach the same level of efficiency without blade pitch control, but the first tests with pitch control confirm there is an improvement potential, with up to 27% relative efficiency gain, bringing the 2D turbine efficiency close to the Betz limit.

The preliminary results from 3D simulations show that high blade aspect ratio $AR = \frac{H}{c}$ is necessary in order to reduce the drop of efficiency between "ideal" 2D turbines and real ones. End-plates may help limiting 3D losses but their size should be minimized in order to limit the added drag.

Further studies using this kind of simulations are needed in order to optimize the efficiency of a Darrieus turbine. More 3D simulations are essential in order to evaluate precisely the drop between 2D results and an hypothetical real turbine, especially turbines with high blade aspect ratios. Other dynamic pitch control functions could also help improve other aspects of a vertical axis turbine, such as self-starting or lower torque ripple [20, 22, 23].

Acknowledgements

Most of the present simulations were computed on the supercomputer Colosse at Université Laval, managed by Calcul Québec and Compute Canada. The authors would like to thank Thomas Kinsey for fruitful discussions and his help with reviewing this manuscript. Financial support from NSERC/DG program is also gratefully aknowledged.

REFERENCES

[1] J. R. Templin. Aerodynamic performance theory for the NRC vertical axis wind turbine. Technical report, NRC Institute for Aerospace Research; National Research Council Canada, 1974.

[2] J. H. Strickland. The darrieus turbine: a performance prediction model using multiple streamtubes. Technical report, Sandia Laboratories, October 1975.

[3] I. Mays and B. A. Holmes. Commercial development of the variable geometry vertical axis windmill. International Power Generation, Surrey, UK, 1979.

[4] W. Grylls, B. Dale, and P. E. Sarre. A theoretical and experimental investigation into the variable pitch vertical axis wind turbine. *Proc. 2nd Int. Symposium on Wind Energy Systems*, E9:101–118, 1978.

[5] E. Williams Beans. Approximate aerodynamic analysis for multi-blade darrieus wind turbine. *Journal of wind engineering and industrial aerodynamics*, 25:131–150, 1987.

[6] I. Paraschivoiu. *Wind Turbine Design with emphasis on Darrieus concept*. Polytechnic International Press, 2002.

[7] S. Armstrong, A. Fiedler, and S. Tullis. Flow separation on a high reynolds number, high solidity vertical axis wind turbine with straight and canted blades and canted blades with fences. *Renewable Energy*, 41:13–22, 2012.

[8] R. Howell, N. Qin, J. Edwards, and N. Durrani. Wind tunnel and numerical study of a small vertical axis wind turbine. *Renewable Energy*, 33:412–422, 2010.

[9] R. Gosselin. Control of flow separation on vertical axis wind turbine blades. Master's thesis, Departement of Mechanical Engineering, University of Sheffield, September 2008.

[10] Y. Li and S. M. Calisal. Three-dimensional effects and arm effects on modeling a vertical axis tidal current turbine. *Renewable Energy*, pages 1–10, 2010.

[11] K. Pope, I. Dincer, and G. F. Naterer. Energy and exergy efficiency comparison of horizontal and vertical axis wind turbines. *Renewable Energy*, 35:2102–2113, 2010.

[12] ANSYS Inc. Ansys fluent 13.0 user's guide, 2010. www.ansys.com.

[13] C. J. S. Ferreira, H. Bijl, G. van Bussel, and G. van Kuik. Simulating dynamic stall in a 2d VAWT: Modeling strategy, verification and validation with particle image velocimetry data. *Journal of Physics*, Conference Series 75, 2007.

[14] S. Wang, D. B. Ingham, L. Ma, M. Pourkashanian, and Zhi Tao. Numerical investigations on dynamic stall of low Reynolds number flows around oscillating airfoils. *Computers & fluids*, 39:1529–1541, 2010.

[15] M. R. Castelli, A. Englaro, and E. Benini. The darrieus wind turbine: Proposal for a new performance prediction model based on CFD. *Energy*, 36:4919–4934, August 2011.

[16] J. Dacles-Mariani, G. G. Zilliac, J. S. Chow, and P. Bradshaw. Numerical/experimental study of a wingtip vortex in the near field. *AIAA Journal*, 33(9):1561–1568, 1995.

[17] J. Dacles-Mariani, D. Kwak, and G. G. Zilliac. On numerical errors and turbulence modeling in tip vortex flow prediction. *International Journal for Numerical Methods in Fluids*, 30:65–82, 1999.

[18] R. E. Sheldahl, P. C. Klimas, and L. V. Feltz. Aerodynamic performance of a 5-meter-diameter darrieus turbine. *AIAA Journal of Energy*, 4(5), September 1980.

[19] C. B. Devaud, J. Weisinger, D. A. Johnson, and E. J. Weckman. Experimental and numerical characterization of the flowfield in the large-scale UW live fire research facility. *International Journal for Numerical Methods in Fluids*, 60:539–564, 2009.

[20] I. Paraschivoiu, O. Trifu, and F. Saeed. H-darrieus wind turbine with blade pitch control. *International Journal of Rotating Machinery*, Volume 2009, 2009.

[21] B. K. Kirke. *Evaluation of self-starting vertical axis wind turbines for stand-alone applications*. PhD thesis, School of Engineering, Griffith University, Gold Coast Campus, April 1998.

[22] B. K. Kirke and L. Lazauskas. Experimental verification of a mathematical model for predicting the performance of a self-acting variable pitch vertical axis wind turbine. *Wind engineering*, 17:58–66, 1993.

[23] S. Sarkar and K. Venkatraman. Influence of pitching angle of incidence on the dynamic stall behavior of a symmetric airfoil. *European Journal of Mechanics B/Fluids*, 27:219–238, 2008.